JOURNAL OF SOLID STATE CHEMISTRY 137, 191–205 (1998)
ARTICLE NO. SC977660

The Systems Ce–Al–(Si, Ge): Phase Equilibria and Physical Properties

H. Flandorfer,* D. Kaczorowski,† J. Gröbner,‡ P. Rogl,* R. Wouters,§ C. Godart,¶,‖ and A. Kostikas**

*Institut für Physikalische Chemie, Universität Wien, A-1090 Wien, Währingerstraße 42, Austria; † W. Trzebiatowski Institute for Low Temperature and Structure Research, Polish Academy of Science, P.O.B. 937, PL-50950 Wroclaw, Poland; ‡ Material Science International, Nobelstraße 15, Postfach 800749, D-70507 Stuttgart, Germany; § Department of Metallurgy and Materials Engineering, Katholieke Universiteit Leuven, de Croylaan 2, B-3001 Heverlee, Belgium; ¶ CNRS, UPR 209, Pl. A. Briand, 92195 Meudon,France; ‖ CNRS, LURE, University of Paris Sud, 91405 Orsay, France; and ** Institute of Materials Science, NCSR, Demokritos, Aghia Paraskevi, Gr-15310 Athens, Greece

Received March 27, 1997; in revised form September 30, 1997; accepted October 13, 1997

The phase relations in the Ce-poor region of the ternary systems Al–Ce–(Ge, Si) were re-established at 600°C for Ce-concentrations up to 33 at.% Ce. The exact phase triangulation and structure determination for both systems were determined by EPMA and X-ray powder diffraction techniques. The homogeneity regions at 600°C were redetermined for the two phases within the section $Ce(Al_xSi_{1-x})_2$: $CeAl_{1.46}Si_{0.54}$ (AlB_2-type) and $CeAl_{0.45-1.28}Si_{1.55-0.72}$ ($\alpha ThSi_2$-type). Besides these two phases, the only compound stable at 600°C in the system Al–Ce–Si was found to be $CeAlSi_2$ with a new structure type. $CeAl_2Si_2$ with the La_2O_2S-type, reported in earlier investigations, was shown to be metastable. Similarly, the existence of the phases reported earlier, "$CeAl_{1.25-1.75}Si_{2.75-2.25}$," "$Ce_2Al_{3.5}Si_{4.5}$," and "$Ce_2Al_3Si_2$," was not confirmed at 500°C or 600°C. $Ce_3Al_4Si_6$ ($Ce_3Al_4Si_6$-type) was obtained in pure form after long-term annealing of melt spun samples at 500°C. For the Al–Ce–Ge system, our investigations at 600°C confirmed the five ternary compounds known from the existing literature. Homogeneity regions and location of the ternary phases were redefined. XAS and magnetic susceptibility measurements revealed a tripositive cerium ground state, $^2F_{5/2}$, in all the compounds studied. $CeAl_{1.2}Si_{0.8}$, $CeAlSi_2$, $Ce_3Al_4Si_6$, and $Ce_2Al_{1.6}Ge_{5.4}$ are antiferromagnets with T_N of 4.2, 3.7, 3.5, and 4.7 K, respectively. In turn, $CeAl_2Si_2$, CeAlGe, and $Ce_2Al_3Ge_4$ order ferromagnetically below 8, 5.6, and 11 K, respectively. The electrical resistivity of all these phases is characteristic of cerium intermetallics with pronounced crystal field effects. © 1998 Academic Press

INTRODUCTION

Several independent investigations dealt with the Ce-poor (≤ 33 at.% Ce) isothermal section of the Ce–Al–Si ternary at 500°C. For details see the critical assessment of literature (1–7) by Rogl (8). A total of four ternary phases were reported to exist: $CeAl_2Si_2$, $CeAl_{1.25-1.75}Si_{2.75-2.25}$, $CeAl_{1.4-0.9}Si_{0.6-1.1}$, and $CeAl_{1.64-1.55}Si_{0.36-0.45}$. Some controversy concerns the region $Ce(Al,Si)_{\sim 4}$, which was claimed to contain the ternary phases $CeAl_{1.25-1.75}Si_{2.75-2.25}$ and $CeAl_2Si_2$. Recently we characterized by ab-initio X-ray powder refinement two hitherto unknown compounds, $CeAlSi_2$ and $Ce_3Al_4Si_6$, both with unique structure types (9).

The Ce-poor (≤ 33 at.% Ce) isothermal section of the Ce–Al–Ge ternary at 500°C, assessed by Schmid-Fetzer (10), is based on previous investigations (5,11,12). Five ternary phases were mentioned: $CeAl_2Ge_2$ (β), $CeAl_{0.5-0.75}Ge_{3.5-3.25}$ (ε), $CeAl_{0.8-1}Ge_{2.2-2}$ (δ), $CeAl_{0.7-1.2}Ge_{1.3-0.8}$ (γ), and $CeAl_{1.5-1.6}Ge_{0.5-0.4}$ (α). Later investigations (13, 14, 15) confirmed the crystal structure of the γ-phase and established two further crystal structures, $Ce_2Al_3Ge_4$ and $Ce_2Al_{1.6}Ge_{5.4}$. Based on this rather incomplete and inconsistent phase equilibria information for both systems, Al–Ce–(Ge, Si), the present work attempts to establish true compound formation and proper phase field distribution, as well as to determine the physical (electrical and magnetic) properties of the ternary compounds.

EXPERIMENTAL

All samples, each about 2g, were synthesized by argon arc melting. The following starting materials were used: Ce, ingot, *m*3*N*, Auer-Remy, Germany; Al, ingots, 99.9%, Johnson and Matthey, Germany; Si, lumps, 99.99%, Johnson and Matthey, Germany; and Ge, pieces, 99.9999%, ABCR, Germany. After melting, the reguli were packed in molybdenum foil, sealed in evacuated silica tubes and heat treated at 600°C. After annealing, the samples were quenched in cold water. Melt spinning under argon atmosphere was performed on selected samples, starting with the corresponding arc melted master alloy. The liquid alloy was ejected through a quartz jet nozzle by pressurized argon and quenched on a cooled copper wheel rotating at a speed of $10–40\ ms^{-1}$.

0022-4596/98 $25.00

Further details of sample preparation and the various X-ray techniques, including Rietveld full matrix, full profile refinements, can be found in a foregoing paper (9). The microstructure of the alloys was inspected by optical microscopy on smooth surfaces prepared by grinding (SiC-paper) and polishing the resin-mounted alloys with diamond pastes to 1/4 μm grain size. Quantitative EMPA was performed on an JEOL 733 Superprobe in Leuven with an energy dispersive X-ray Si(Li) detector system by Tracor Northern, employing the ZAF correction program (16). Operation conditions were 15 kV acceleration voltage, 2×10^{-9} A beam current, and a net counting time of 100 s.

X-ray absorption measurements were carried out at room temperature and 10 K at the French synchrotron radiation facility of LURE using the X-ray beam delivered by the DCI storage ring, working on the EXAFS2 station at 1.85 GeV–250 mA. For further details see, i.e., Refs. 17–19. Experiments were made in the range 5640–5820 eV around the L_{III} edge of Ce. Magnetization and dc-magnetic susceptibility measurements were performed in the temperature range 1.7–300 K in applied fields up to 50 kOe using a Quantum Design MPMS-5 superconducting quantum interference device magnetometer. Electrical resistivity measurements were carried out on bar-shaped specimens in the temperature range 4.5–300 K by conventional dc four probe technique.

BINARY SYSTEMS

The binary systems Al–Si, Al–Ce, Ce–Si, and Ce–Ge are accepted from (20).

RESULTS AND DISCUSSION

A. The Ce−Al−Si system

A.1. Solid Phases

From the four ternary phases, shown in the assessment (8) to appear in the 500°C isothermal section of the Al–Ce–Si system, our results confirm only the existence of phases with the $\alpha ThSi_2$- and AlB_2-type structure (Fig. 1). $CeSi_2$ ($\alpha ThSi_2$-type) dissolved up to 5 at.% Al, followed by a two-phase region or a miscibility gap between 5 and 15 at.% Al. Further substitution of Si by Al again stabilizes this structure type up to about 43 at.% Al. This phase was in equilibrium with the AlB_2-type phase of the approximate composition $Ce_{33}Al_{49}Si_{18}$. The homogeneity region of the AlB_2-type phase was rather small, as the composition $Ce_{33}Al_{47}Si_{20}$ was found in equilibrium with $CeAl_2$ at 2.1 at.% Si. These two limiting compositions of the AlB_2-type phase were slightly different but in the reverse than expected. However, the difference was within the error

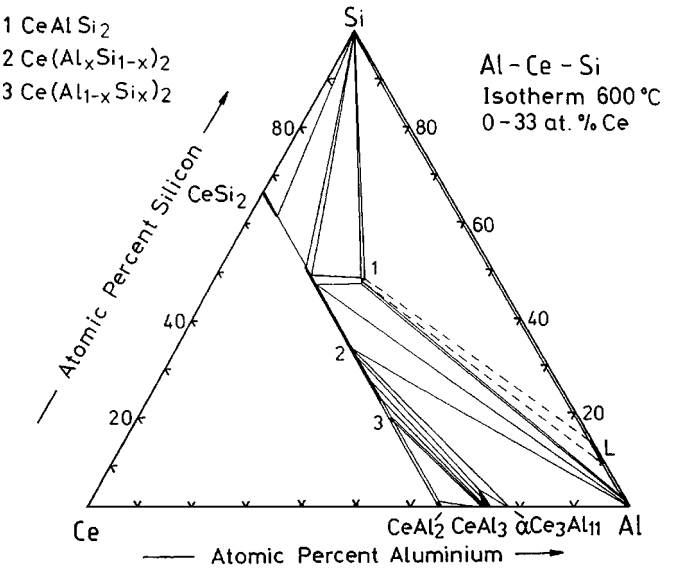

FIG. 1. Partial isothermal section of the ternary Al–Ce–Si system at 600°C.

of EMPA measurements, and we therefore consider the AlB_2-type phase as a ternary compound with a very small homogeneity range. Whereas the $\alpha ThSi_2$-type phase was observed to melt congruently, the AlB_2-type phase appeared from the arc in combination with $CeAl_2$ ($MgCu_2$-type) as a secondary phase, which even after prolonged annealing at 600°C or 800°C did not disappear. Shifting the composition toward the ternary $\alpha ThSi_2$-type phase, $CeAl_2$ disappeared completely after prolonged annealing (672 h), but the $\alpha ThSi_2$-type structure was obtained in addition. This implies a very small two-phase region between the $\alpha ThSi_2$-type and the AlB_2-type. $CeAl_3$ dissolved 3.5 at.% Si, while αCe_3Al_{11} showed almost no ternary solid solubility.

Along the section $Ce(Al, Si)_4$, the compound $CeAl_2Si_2$ with the La_2O_2S-type structure, reported in Refs. 6 and 7, was never obtained in pure form from arc melted samples, but usually together with $Ce(Al_xSi_{1-x})_2$, $\alpha ThSi_2$-type, and Al. $CeAl_2Si_2$ disappeared after annealing at 700, 600, or 500°C for 168 h and may therefore be considered to be a metastable phase. Thus, the only stable compound in this region after annealing between 600 and 650°C is $CeAlSi_2$ (see Table 1 and Fig. 1). Above 650°C, $CeAlSi_2$ decomposed into $Ce(Al_xSi_{1-x})_2$, Al, and Si. Below 600°C, after 336 h of annealing, another phase with the approximate composition $CeAl_{1.33}Si_2$ ($Ce_3Al_4Si_6$) appeared, with $CeAlSi_2$ still present. Suspecting a high-temperature behavior of $CeAl_2Si_2$, we tried stabilization by melt spinning. Whereas in most cases, melt spinning of $CeAl_2Si_2$ yielded a three phase mixture $Ce(Al_xSi_{1-x})_2 + Al + Si$, which also prevailed after annealing at 700°C for 168 h, a few experiments yielded almost single phase $CeAl_2Si_2$. Melt spun samples of $CeAl_2Si_2$, after

annealing at 500°C for 168 h, resulted in pure $Ce_3Al_4Si_6$. The crystal structures of both new compounds, $CeAlSi_2$ and $Ce_3Al_4Si_6$, were recently determined (9). The phases "$CeAl_{1.25-1.75}Si_{2.75-2.25}$" (6), "$Ce_2Al_{3.5}Si_{4.5}$" (2,3), and "$Ce_2Al_3Si_2$" (1) could not be found and may not be pertinent to the Al–Ce–Si ternary.

The full profile, full matrix Rietveld refinement of an alloy with the $ThSi_2$-type structure, $CeAl_{1.2}Si_{0.8}$, is presented in Table 2. No extra lines and very low residual values confirmed the absence of superstructures.

A.2. Isothermal Section

Figure 1 shows the partial isothermal section ($\leq$33 at.% Ce) at 600°C, characterized by the ternary compound $CeAlSi_2$ with a rather restricted homogeneous region and the extended solid solubility of the $ThSi_2$-type phase. Crystallographic data evaluated by X-ray investigation and EMPA results of solid phases are listed in Table 3. The BSE micrograph of $Ce_{12}Al_{83}Si_5$ in Fig. 2a clearly shows the three-phase equilibrium: $Al + \alpha Ce_3Al_{11} + Ce(Al_{1-x}Si_x)_2$

TABLE 1
Crystallographic Data of Alloys Al–Ce–Si

Alloy nominal compositions at.%	Heat treatment	Phase analysis	Structure type	Space group	Unit cell dimensions in nm[a]			
					a	*c*	*V* (nm^3)	*c*/*a*
$Ce_{20}Al_{40}Si_{40}$	arc	$CeAl_2Si_2$	La_2O_3	$P\bar{3}m1$	0.4217(0)	0.6895(1)	0.1062	1.6350
		$Ce(Al_xSi_{1-x})_2$	$\alpha ThSi_2$	$I4_1/amd$	0.4234(0)	1.4308(1)	0.2565	3.3793
		Al	Cu	$Fm\bar{3}m$	traces			
	melt spun	$Ce(Al_xSi_{1-x})_2$	$\alpha ThSi_2$	$I4_1/amd$	0.4236(0)	1.4233(4)	0.2554	3.3600
		Al	Cu	$Fm\bar{3}m$	0.4056(1)		0.0667	
		Si	C_{dia}	$Fd\bar{3}m$	0.5438(1)		0.1608	
	700°C	$Ce(Al_xSi_{1-x})_2$	$\alpha ThSi_2$	$I4_1/amd$	0.4235(0)	1.4237(4)	0.2554	3.3617
		Al	Cu	$Fm\bar{3}m$	0.4052(0)		0.0665	
		Si	C_{dia}	$Fd\bar{3}m$	0.5434(1)		0.1605	
	600°C	$CeAlSi_2$	$CeAlSi_2$	$P\bar{3}m1$	0.4172(0)	1.1216(6)	0.1691	2.6884
		Al	Cu	$Fm\bar{3}m$	0.4049(0)		0.0664	
		Si	C_{dia}	$Fd\bar{3}m$	0.5429(1)		0.1600	
	500°C	$CeAl_{1.33}Si_2$	$Ce_3Al_4Si_6$	$P\bar{3}m1$	0.4189(0)	1.8111(5)	0.2753	4.3234
		$CeAlSi_2$	$CeAlSi_2$	$P\bar{3}m1$	0.4175(1)	1.1230(9)	0.1695	2.6898
		Al	Cu	$Fm\bar{3}m$	0.4047(0)		0.0663	
		Si	C_{dia}	$Fd\bar{3}m$	traces			
$Ce_{20}Al_{30}Si_{50}$	arc	$Ce(Al_xSi_{1-x})_2$	$\alpha ThSi_2$	$I4_1/amd$	0.4222(0)	1.4173(7)	0.2527	3.3568
		Al	Cu	$Fm\bar{3}m$	0.4050(0)		0.0664	
		Si	C_{dia}	$Fd\bar{3}m$	0.5430		0.1601	
	600°C	$CeAlSi_2$	$CeAlSi_2$	$P\bar{3}m1$	0.4171(1)	1.1218(5)	0.1690	2.6895
		Al	Cu	$Fm\bar{3}m$	traces			
		Si	C_{dia}	$Fd\bar{3}m$	traces			
	500°C	$CeAl_{1.33}Si_2$	$Ce_3Al_4Si_6$	$P\bar{3}m1$	0.4189(0)	1.8118(4)	0.2754	4.3250
		$CeAlSi_2$	$CeAlSi_2$	$P\bar{3}m1$	0.4170(0)	1.1213(1)	0.1689	2.6888
		$Ce(Al_xSi_{1-x})_2$	$\alpha ThSi_2$	$I4_1/amd$	0.4231(0)	1.4312(1)	0.2562	3.3827
$Ce_{20}Al_{35}Si_{45}$	600°C	$CeAlSi_2$	$CeAlSi_2$	$P\bar{3}m1$	0.4171(1)	1.1206(8)	0.1688	2.6867
		Al	Cu	$Fm\bar{3}m$	0.4052(0)		0.0665	
		Si	C_{dia}	$Fd\bar{3}m$	0.5434(1)		0.1605	
$Ce_{20}Al_{55}Si_{45}$	600°C	$CeAlSi_2$	$CeAlSi_2$	$P\bar{3}m1$	0.4174(2)	1.1219(9)	0.1692	2.6880
		Al	Cu	$Fm\bar{3}m$	0.4048(1)		0.0663	
		Si	C_{dia}	$Fd\bar{3}m$	traces			
$Ce_{33.3}Al_{38.3}Si_{70.6}$	arc	$Ce(Al_xSi_{1-x})_2$	$\alpha ThSi_2$	$I4_1/amd$	0.4267(1)	1.4679(5)	0.2673	3.4401
	600°C	$Ce(Al_xSi_{1-x})_2$	$\alpha ThSi_2$	$I4_1/amd$	0.4265(1)	1.4680(5)	0.2671	3.4419
$Ce_{33.3}Al_{53.3}Si_{13.4}$	arc	$Ce(Al_{1-x}Si_x)_2$	AlB_2	$P6/mmm$	0.4310(3)	0.4304(4)	0.0692	0.9986
		$CeAl_2$	Cu_2Mg	$Fd\bar{3}m$	0.8075(3)		0.5264	
	600°C	$Ce(Al_{1-x}Si_x)_2$	AlB_2	$P6/mmm$	0.4314(1)	0.4312(1)	0.0695	0.9996
		$CeAl_2$	Cu_2Mg	$Fd\bar{3}m$	0.8071(2)		0.5257	
	800°C	$Ce(Al_{1-x}Si_x)_2$	AlB_2	$P6/mmm$	0.4311(0)	0.4309(2)	0.0693	0.9995
		$CeAl_2$	Cu_2Mg	$Fd\bar{3}m$	0.8067(2)		0.5250	

[a]Standard deviation (e.s.d.) is given in parentheses; zero value means e.s.d. is lower than 0.5.

($\alpha ThSi_2$-type). The BSE micrograph and EMPA data of the three-phase alloy $Ce_{20}Al_{10}Si_{70}$ in Fig. 2b, however, confirm the well established phase field: $Si + CeSi_{2-x}Al_x + Ce(Al_xSi_{1-x})_2$, the difference in the electron density of the two $ThSi_2$-type phases being too small to be recognized clearly from the graph.

B. The Ce–Al–Ge System

B.1. Solid Phases

The assessment of the Al–Ce–Ge system (10) shows five different ternary phases in the 500°C isothermal section. The results of our investigations at 600°C (Fig. 3) confirm the existence of all these phases. $CeGe_{2-x}$ ($\alpha ThSi_2$ type) solves up to 4 at.% Al. A two-phase region (or miscibility gap) between the two isostructural $ThSi_2$ phases occurs between 4 at.% and 26 at.% Al. Further substitution of Ge by Al again stabilizes this structure type up to at least 44 at.% Al. $CeAl_3$ solves 2.6 at.% Ge, whereas the ternary solid solubility of $CeAl_2$ and αCe_3Al_{11} can be neglected. $CeAl_2$ is observed in equilibrium with the AlB_2-type $Ce_{33.3}Al_{50}Ge_{17.7}$, whereas the phase relations between the $\alpha ThSi_2$-type phase ($\geq$44 at.% Al) and the AlB_2-type phase (18 at.% Ge) could not be derived with certainty. In analogous fashion to the Ce–Al–Si system, a very small two-phase region between the $\alpha ThSi_2$-type and AlB_2-type phases or a second order transformation is considered.

The phases $CeAl_2Ge_2$ and $Ce_2Al_3Ge_4$ (15), the latter probably corresponding to the δ-phase of (11), were found with very restricted homogeneity ranges. Several attempts to synthesize $CeAl_2Ge_2$ in pure form failed. Arc melting as well as melt spinning yielded multiphase alloys containing $CeAl_2Ge_2$ and $Ce_2Al_3Ge_4$. In some alloys $CeAl_2Ge_2$ seemed to decompose during annealing (see BSE micrograph in Fig. 4a), whereas other alloys showed this phase in a stable equilibrium (see BSE micrograph in Fig. 4b). The homogeneity range of the monoclinic phase $Ce_2Al_xGe_{7-x}$ (15), probably corresponding to the ε-phase (11), was determined by EMPA to be in the range $0.73 \leq x \leq 1.27$ (Fig. 5).

X-ray intensity patterns of selected alloys representing the five ternary phases mentioned above were refined employing the Rietveld method to reveal precise atom coordinates, atom site distribution, occupancies, and interatomic distances. Occupation factors were refined in all cases and nicely corresponded to the EMPA data of nominal compositions. Due to the usually strong correlations with the temperature factors B_{ij}, the occupancies were kept fixed in the final runs to refine the B_{ij} values. The results are presented in Tables 4–8 and confirm the crystallographic symmetry and isotypism of these compounds with the structure types mentioned above (14, 15).

TABLE 2
Crystallographic Data of $CeAl_{1.2}Si_{0.8}$ Quenched from 600°C

Method	Full profile refinement of room temperature X-ray powder diffraction data Number of reflections used in refinement: 94, $20^\circ \leq 2\theta \leq 100^\circ$
Lattice parameters	$a = 0.42741(1)$ nm, $c = 1.4732(1)$ nm, $V = 0.2691$ nm^3, $c/a = 3.4468$
Structure type	$\alpha ThSi_2$
Space group	$I4_1/amd$–D_{4h}^{19}, No. 141, origin at $\bar{1}$, $Z = 4$
Residual values	$R_I = 0.046$, $R_F = 0.029$, $R_P = 0.091$, $R_{wP} = 0.114$

Atom parameters

Atom	Site	x	y	z	B in 10^{-2} nm^2	Occupation
Ce	4a	0	0.75	0.125	0.73(3)	1
(Al, Si)	8e	0	0.25	0.2941(2)	1.5(1)	(0.6 Al + 0.4 Si)

Preferred orientation: 0.053(4) for [001]

Interatomic distance (in nm) e.s.d. <0.0004

Central Atom: Ce		Central Atom: (Al, Si)	
Ligand Atom	Distance	Ligand Atom	Distance
8 (Al, Si)	0.3249	1 (Al, Si)	0.2384
4 (Al, Si)	0.3282	2 (Al, Si)	0.2501
4 Ce	0.4258	4 Ce	0.3249
4 Ce	0.4274	2 Ce	0.3282

TABLE 3
Crystallographic and EPMA Data of Alloys Al–Ce–Si Quenched from 600°C

Alloy nominal compositions, at.%	Phase analysis	Structure type	Space group	Unit cell dimensions in nm[a]					EPMA results in at. %			
				a	*b*	*c*	*V* (nm^3)	*c*/*a*	Ce	Al	Si	∑m.%
$Ce_{20}Al_{10}Si_{70}$	$Ce(Al_xSi_{1-x})_2$	$\alpha ThSi_2$	$I4_1/amd$	0.4234(1)		1.4453(6)	0.2591	3.2990	33.1	16.3	50.6	102.2
	$CeSi_2$	$\alpha ThSi_2$	$I4_1/amd$	0.4234(2)		1.3968(8)	0.2504	3.3793	32.9	4.8	62.3	102.3
	Si	C_{dia}	$Fd\bar{3}m$	0.5431(0)			0.1602		0.1	0.0	99.9	99.6
$Ce_{32}Al_{52}Si_{16}$	$Ce(Al_{1-x}Si_x)_2$	AlB_2	$P6/mmm$	0.4309(1)		0.4308(3)	0.0693	0.9997	33.2	48.5	18.3	100.2
	$Ce(Al_xSi_{1-x})_2$	$\alpha ThSi_2$	$I4_1/amd$	0.4299(1)		1.4876(7)	0.2749	3.4604	33.7	43.6	22.8	100.8
	$CeAl_3$	Ni_3Sn	$P6_3/mmc$	0.6550(1)		0.4621(1)	0.1717	0.7055	25.9	74.1	0.0	100.5
$Ce_{18}Al_{75}Si_7$	$Ce(Al_xSi_{1-x})_2$	$\alpha ThSi_2$	$I4_1/amd$									
	Ce_3Al_{11}	La_3Al_{11}	$Immm$									
$CeAlSi_2$	$CeAlSi_2$	$CeAlSi_2$	$P\bar{3}m1$	0.4169(1)		1.1217(4)	0.1689	2.6903	24.8	26.8	48.5	102.1
	$Ce(Al_xSi_{1-x})_2$	$\alpha ThSi_2$	$I4_1/amd$	0.4238(5)		1.4452(6)	0.2596	3.4104	33.3	17.2	49.5	102.3
	Si	C_{dia}	$Fd\bar{3}m$	0.5426			0.1597		0.2	0.3	99.5	101.4
$CeAl_{1.5}Si_2$	$CeAlSi_2$	$CeAlSi_2$	$P\bar{3}m1$									
	$Ce_3Al_4Si_6$	$Ce_3Al_4Si_6$	$P\bar{3}m1$									
	$Ce(Al_xSi_{1-x})_2$	$\alpha ThSi_2$	$I4_1/amd$									
	Si	C_{dia}	$Fd\bar{3}m$									
$CeAl_{1.6}Si_{0.4}$	$Ce(Al_xSi_{1-x})_2$	AlB_2	$P6/mmm$	0.4307(0)		0.4308(1)	0.0692	1.0001	34.1	45.9	20.0	100.6
	$CeAl_2$	Cu_2Mg	$Fd\bar{3}m$	0.8065(1)			0.5246		34.4	63.5	2.1	100.4
	$CeAl_3$	Ni_3Sn	$P6_3/mmc$	traces					26.5	73.5	0.0	98.8
$Ce_{33.3}Al_{45.7}Si_{21}$	$Ce(Al_xSi_{1-x})_2$	$\alpha ThSi_2$	$I4_1/amd$	0.4295(1)		1.4880(9)	0.2744	3.4646	33.8	43.1	23.1	101.1
	$Ce(Al_xSi_{1-x})_2$	AlB_2	$P6/mmm$	0.4301(2)		0.4311(3)	0.0691	1.0023	34.1	48.0	17.9	100.5
$Ce_{32}Al_{46}Si_{22}$	$Ce(Al_xSi_{1-x})_2$	$\alpha ThSi_2$	$I4_1/amd$	0.4282(7)		1.4790(4)	0.2712	3.4537	34.1	39.3	26.6	101.3
	$CeAl_3$	Ni_3Sn	$P6_3/mmc$	0.6545(5)		0.4612(3)	0.1711	0.7048	25.8	71.9	2.3	99.8
$Ce_{25}Al_{72}Si_3$	$CeAl_3$	Ni_3Sn	$P6_3/mmc$	0.6538(2)		0.4603(2)	0.1704	0.7041	25.8	70.7	3.5	99.5
	Ce_3Al_{11}	La_3Al_{11}	$Immm$	0.4400(2)	1.3013(5)	1.0082(2)	0.5772		22.2	77.3	0.0	100.7
	$Ce(Al_xSi_{1-x})_2$	$\alpha ThSi_2$	$I4_1/amd$	traces					33.3	35.7	31.0	100.7
$Ce_{12}Al_{83}Si_5$	Ce_3Al_{11}	La_3Al_{11}	$Immm$	0.4386(1)	1.3028(5)	1.0069(6)	0.5753		22.0	78.0	0.0	98.6
	$Ce(Al_xSi_{1-x})_2$	$\alpha ThSi_2$	$I4_1/amd$	0.4254(1)		1.4615(3)	0.2645	3.4353	33.4	33.2	33.4	100.8
	Al	Cu	$Fm\bar{3}m$	0.4049(1)			0.0664		0.1	99.9	0.0	98.4
$Ce_{10}Al_{35}Si_{55}$	$CeAlSi_2$	$CeAlSi_2$	$P\bar{3}m1$	0.4170(1)		1.1224(7)	0.1690	2.6914	24.7	27.5	47.8	101.5
	Al	Cu	$Fm\bar{3}m$	0.4052(1)			0.6650		0.0	98.1	1.9	100.1
	Si	C_{dia}	$Fd\bar{3}m$	0.5432(1)			0.1603		0.1	0.0	99.9	106.4
$Ce_{25}Al_{35}Si_{40}$	$CeAlSi_2$	$CeAlSi_2$	$P\bar{3}m1$	0.4173(2)		1.1226(3)	0.1693	2.6903	24.7	27.9	47.4	101.8
	$Ce(Al_xSi_{1-x})_2$	$\alpha ThSi_2$	$I4_1/amd$	0.4240(3)		1.4388(7)	0.2586	3.3935	33.3	19.2	47.6	101.5
	Al	Cu	$Fm\bar{3}m$	0.4052(2)			0.6654		0.0	97.9	2.1	100.0

[a]Standard deviation (e.s.d.) is given in parentheses; zero value means e.s.d. is lower than 0.5.

B.2. Isothermal Section

Figure 3 shows the phase field distribution in the partial isothermal section up to 33 at.% Ce at 600°C. The major difference to the hitherto accepted phase triangulation in the Ce–Al–Ge system at 500°C (10) is the absence of a homogeneous region for $Ce_2Al_3Ge_4$ (earlier δ-phase), as well as the new locations of the δ-, and ε-phases. Figures 5a and 5b show two BSE micrographs of the alloys $Ce_{23}Al_7Ge_{70}$, revealing a three-phase equilibrium Ge + $CeGe_{2-x}$ (at 64 at.% Ge) + $Ce_2Al_{0.8}Ge_{6.2}$, and $Ce_{20}Al_{70}Ge_{10}$ (three-phase equilibrium: Al + αCe_3Al_{11} + $Ce(Al_xGe_{1-x})_2$ at 35.5% Al). Crystallographic data evaluated by X-ray investigation and EMPA results of solid phases are listed in Table 9.

C. Magnetic Properties

Results on the magnetic properties of the compounds and alloys investigated are summarized in Figs. 6–12 and discussed in detail for each compound. Paramagnetism at temperatures above about 150 K generally was observed to follow a Curie Weiss law corresponding to a tripositive gound state of Ce with an ideal paramagnetic moment of 2.54 μ_B.

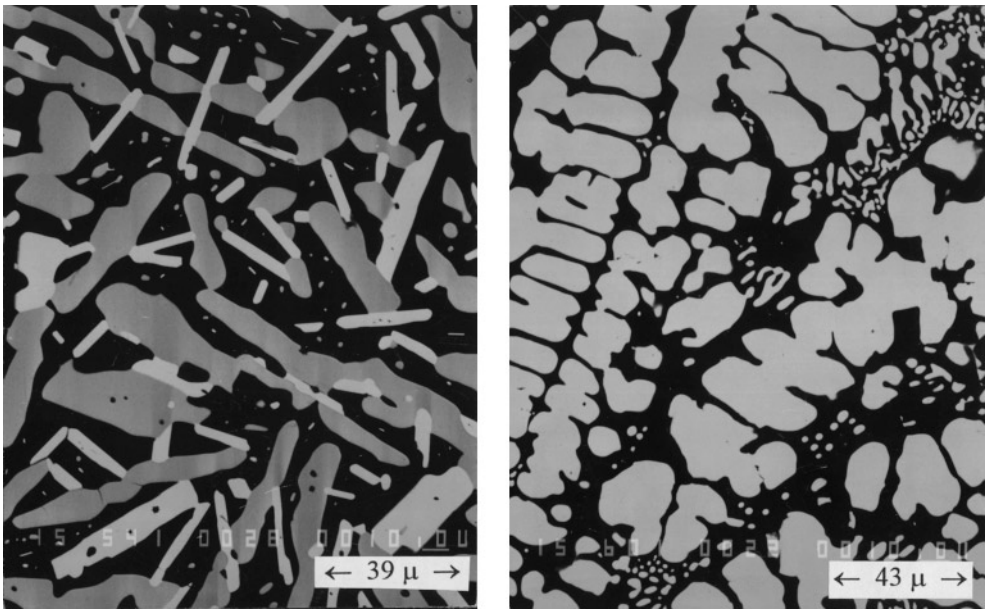

FIG. 2. BSE micrograph of a) $Ce_{12}Al_{83}Si_5$ (bright dendrites ⇒ $Ce(Al_xSi_{1-x})_2$, grey ⇒ Ce_3Al_{11}, dark matrix ⇒ Al) and b) $Ce_{20}Al_{10}Si_{70}$ (bright crystals ⇒ $Ce(Al_xSi_{1-x})_2$ and $(Ce,Al)Si_2$, dark matrix ⇒ Si) annealed and quenched from 600°C.

$CeAl_{1.2}Si_{0.8}$ ($\alpha ThSi_2$ type). In contrast to earlier observations by Dhar et al. (21, 22), who claimed for this compound a ferromagnetic ordering below 4.2 K, the characteristic maximum in our low temperature susceptibility data as a function of the magnetic field (0.5, 1, 5 kOe, see Fig. 6) suggests instead antiferromagnetic order below $T_N = 4.2$ K. A further argument for the antiferromagnetic ground state comes from the behavior of the magnetization vs magnetic field, which at 1.7 K varies linearly up to 5 kOe, followed by a metamagnetic transition. At 50 kOe the magnetization was 23 emu/g with a tendency to magnetic saturation ($\sigma \approx 0.8\ \mu_B$). The deviations below 120 K from paramagnetic Curie-Weiss behaviour ($\mu_{eff} = 2.58\ \mu_B$, $\Theta_P = -13.4$ K) are due to crystal field effects.

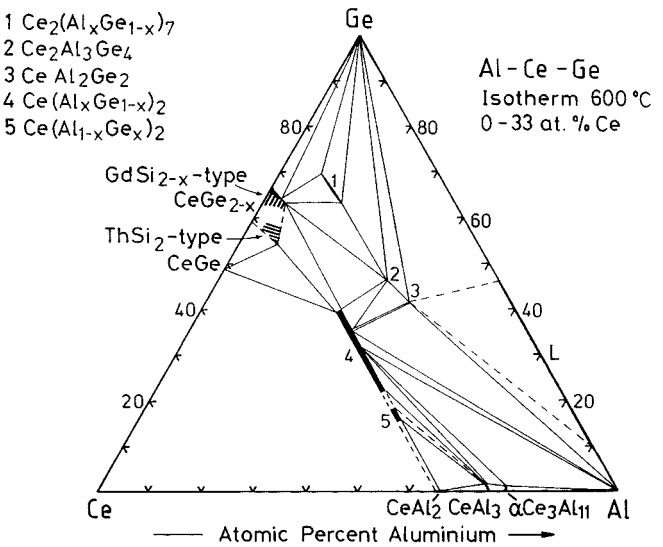

FIG. 3. Partial isothermal section of the ternary Al–Ce–Ge system at 600°C.

$CeAlSi_2$ ($CeAlSi_2$ type). Susceptibility vs temperature and magnetization vs magnetic field (Fig. 7) reveal antiferromagnetic ordering below 3.7 K and a metamagnetic transition at 7 kOe (at 1.7 K). Magnetization at 50 kOe is small (0.65 emu/g) and rather far from saturation. Paramagnetic Curie-Weiss parameters in the range 20–300 K are: $\mu_{eff} = 2.49\ \mu_B$ and $\Theta_P = -19$ K.

$CeAl_2Si_2$ ($CaAl_2Si_2$ type). Susceptibility and magnetization data (Fig. 8) indicate ferromagnetic ordering below $T_c = 8$ K. The large values of the susceptibility, a strong curvature of $\chi^{-1}(T)$ and a peculiar behavior of σ vs B are probably due to ferromagnetic impurities introduced during preparation or handling of the specimens. A rather large amount of this impurity hampered any analysis of the susceptibility data.

$Ce_3Al_4Si_6$ ($Ce_3Al_4Si_6$ type). This compound exhibits antiferromagnetism below $T_N = 3.5$ K with a metamagnetic transition at 8 kOe (Fig. 9). The sample was slightly contaminated by a ferromagnetic impurity, probably the same as observed in $CeAl_2Si_2$. In this case, however, it was possible to correct the measured susceptibility for the impurity content. For that reason, $\chi(T)$ measurements were performed in a field of 5 T and the results were corrected by

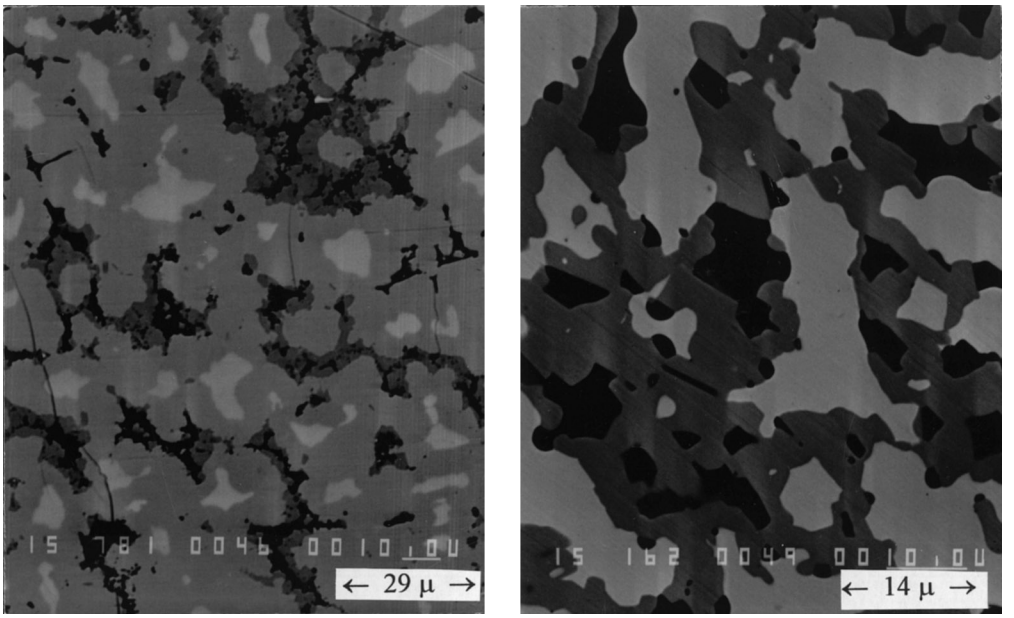

FIG. 4. BSE micrograph of a) $Ce_{24}Al_{34}Ge_{42}$ (bright spots $\Rightarrow Ce(Al_xGe_{1-x})_2$, light grey $\Rightarrow Ce_2Al_3Ge_4$, dark grey matrix $\Rightarrow CeAl_2Ge_2$, decomposing) and b) $Ce_{23}Al_{45}Ge_{32}$ (bright $\Rightarrow Ce(Al_xGe_{1-x})_2$, dark grey $\Rightarrow CeAl_2Ge_2$, black matrix $\Rightarrow$ Al) annealed and quenched from 600°C.

subtracting the saturation magnetization of the impurity, which was determined from σ vs B taken at 300 K. The so-derived susceptibility curve follows the Curie-Weiss law above 20 K with the parameters: $\mu_{eff} = 2.23\ \mu_B$ per Ce atom and $\Theta_P = -8$ K.

CeAlGe ($\alpha ThSi_2$ type). Whereas magnetization vs temperature and field strongly suggest soft ferromagnetic behavior with an ordering temperature of $T_c = 5.6$ K (Fig. 10), a Curie-Weiss fit of the measured susceptibility reveals a negative paramagnetic Curie temperature ($\mu_{eff} = 2.38\ \mu_B$, $\Theta_P = -18$ K). At 50 kOe and 1.7 K the magnetization was 18 emu/g close to magnetic saturation ($\sigma \approx 0.82\ \mu_B$). The deviations from paramagnetic Curie-Weiss behavior below 150 K are due to crystal field effects. Immediately after measurement, the elemental composition of the sample was

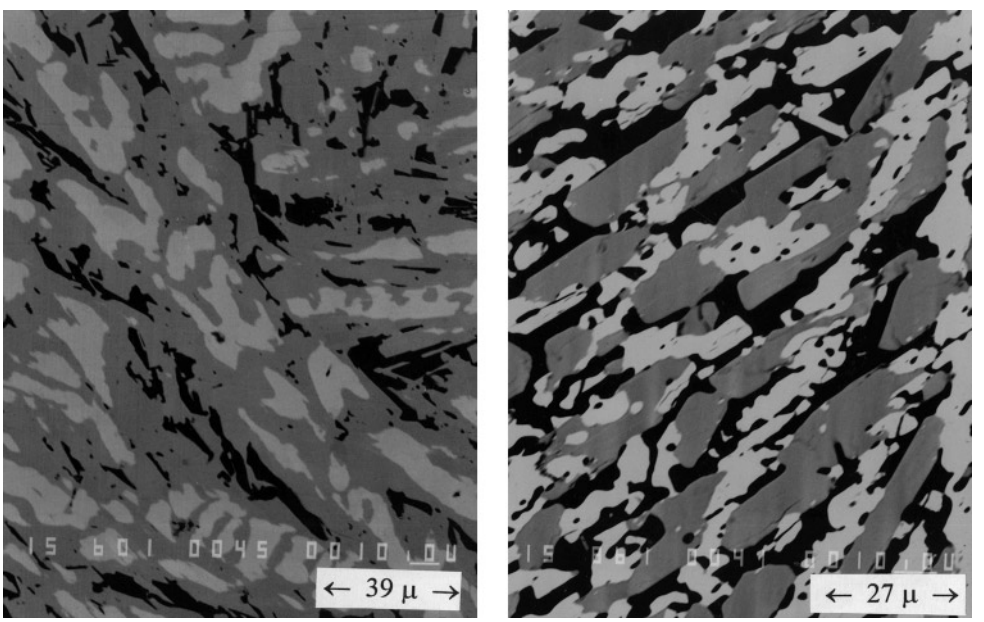

FIG. 5. BSE micrograph of a) $Ce_{23}Al_7Ge_{70}$ (bright $\Rightarrow Ce_2Al_{0.8}Ge_{6.2}$, light grey $\Rightarrow Ce_3Ge_5$, dark matrix $\Rightarrow$ Ge) and b) $Ce_{20}Al_{70}Ge_{10}$ (bright $\Rightarrow Ce(Al_xGe_{1-x})_2$, grey $\Rightarrow Ce_3Al_{11}$, black matrix $\Rightarrow$ Al) annealed and quenched from 600°C.

TABLE 4
Crystallographic Data of $Ce(Al_{0.81}Ge_{0.19})_2$ Quenched from 600°C

Method	Full profile refinement of room temperature X-ray powder diffraction data Number of reflections used in refinement: 56, $20^\circ \le 2\theta \le 100^\circ$
Lattice parameters[a]	$a = 0.4353(1)$ nm, $c = 0.4309(1)$ nm, $V = 0.70718$ nm^3, $c/a = 0.9899$
Structure type	AlB_2
Space group	$P6/mmm$–D^1_{6h}, No. 191, origin at $\bar{1}$, $Z = 2$
Residual values	$R_I = 0.093$, $R_F = 0.069$, $R_P = 0.172$, $R_{wP} = 0.206$

Atom parameters

Atom	Site	x	y	z	B in 10^{-2} nm^2	Occupation
Ce	1a	0	0	0	0.65(5)	1
(Al, Ge)	2d	0.3333	0.6667	0.5	3.9(2)	0.81(1)Ge + 0.19Al

Interatomic distances (in nm) e.s.d. < 0.0004

Central Atom: Ce		Central Atom (Ge, Al)	
Ligand Atom	Distance	Ligand Atom	Distance
4 Ge	0.3310	2 Ge	0.2513
4 Al	0.3310	2 Al	0.2513
8 Ge	0.3311	Ge	0.2514
8 Al	0.3311	Al	0.2514
2 Ce	0.4309	2 Ce	0.3310
6Ce	0.4353	4 Ce	0.3311

Second Phase	Small amounts of $CeAl_2$
Lattice parameters	$a = 0.8065(3)$ nm, $V = 0.5346$ nm^3
Structure type	Cu_2Mg
Space group	$Fd\bar{3}m$–O^7_h, No. 227, Origin at $\bar{1}$, $Z = 4$
Residual values	$R_I = 0.119$, $R_F = 0.062$

[a] Lattice parameters determined from Guinier film.

TABLE 5
Crystallographic Data of CeAlGe Quenched from 600°C

Method	Full profile refinement of room temperature X-ray powder diffraction data Number of reflections used in refinement: 94, $20^\circ \le 2\theta \le 100^\circ$
Lattice parameters[a]	$a = 0.4250(1)$ nm, $c = 1.4711(4)$ nm, $V = 0.27012$ nm^3, $c/a = 3.4333$
Structure type	$\alpha ThSi_2$
Space group	$I4_1/amd$–D^{19}_{4h}, No. 141, origin at $\bar{1}$, $Z = 4$
Residual values	$R_I = 0.077$, $R_F = 0.057$, $R_P = 0.15$, $R_{wP} = 0.197$

Atom parameters

Atom	Site	x	y	z	B in 10^{-2} nm^2	Occupation
Ce	4a	0	0.75	0.1250	0.74(4)	1
(Ge, Al)	8e	0	0.25	0.2916(2)	1.9(3)	0.5(1) Ge + 0.5 Al

Interatomic distance (in nm) e.s.d. < 0.0005

Central Atom: Ce		Central Atom: (Ge, Al)	
Ligand Atom	Distance	Ligand Atom	Distance
4 (Ge, Al)	0.3255	2 (Ge, Al)	0.2454
8 (Ge, Al)	0.3269	4 (Ge, Al)	0.2468
4 Ce	0.4257	2 Ce	0.3255
4 Ce	0.4285	4 Ce	0.3269

[a] Lattice parameters determined from Guinier film.

TABLE 6
Crystallographic Data for $CeAl_2Ge_2$ Quenched from 600°C

Method	Full profile refinement of room temperature X-ray powder diffraction data (flat specimen) Number of reflections used in refinement: 178, $12^\circ \leq 2\theta \leq 100^\circ$
Lattice parameters	$a = 0.42830(1)$ nm, $c = 0.69254(2)$, $V = 0.1100$ nm^3
Structure type	La_2O_2S
Space group	$P\bar{3}m1$–D_{3d}^3, No. 164, origin at $\bar{1}$, $Z = 1$
Residual values	$R_I = 0.045$, $R_F = 0.027$, $R_P = 0.096$, $R_{wP} = 0.126$

Atom parameters

Atom	Site	x	y	z	B in 10^{-2} nm^2	Occupation
Ce	1a	0	0	0	0.94(5)	1
Ge	2d	1/3	2/3	0.2706(3)	0.75(7)	1
Al	2d	1/3	2/3	0.6384(7)	1.3(2)	1

Interatomic distances (in nm) e.s.d < 0.0007

Central Atom: Ce

Ligand Atom	Distances
6 Ge	0.3103
6 Al	0.3519
6 Ce	0.4283

Central Atom: Ge

Ligand Atom	Distances
1 Al	0.2547
3 Al	0.2552
3 Ce	0.3103
3 Ge	0.4027
6 Ge	0.4283

Central Atom: Al

Ligand Atom	Distances
1 Ge	0.2547
3 Ge	0.2552
3 Al	0.3129
3 Ce	0.3519
6 Al	0.4283

Secondary Phase	Small amounts of $Ce_2Al_3Ge_4$
Lattice parameters	$a = 0.60882(3)$ nm, $b = 1.5065(1)$ nm, $c = 0.79829(4)$ nm, $V = 0.7322$ nm^3
Structure type	$Ba_2Cd_3Bi_4$
Space group	$Cmca$–D_{2h}^{18}, No. 64, origin at $\bar{1}$, $Z = 4$
Residual values	$R_I = 0.108$, $R_F = 0.067$

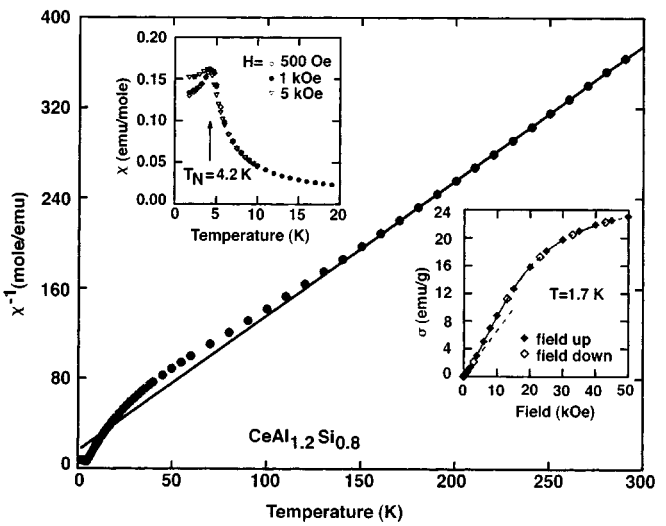

FIG. 6. Temperature variation of the inverse magnetic susceptibility for $CeAl_{1.2}Si_{0.8}$. The solid line is a fit of the experimental data to the Curie-Weiss law. Left inset shows the low temperature dependence of the susceptibility measured at 0.5, 1, and 5 kOe. Right inset shows field dependence of the magnetization measured at 1.7 K with increasing magnetic field (filled symbols) and decreasing field (open symbols). The dashed line represents the linear dependency $\sigma(H)$.

confirmed by EDAX in order to rule out any confusion with isotypic Si-containing samples. This was particularly done in view of the report by Dhar *et al.* (21, 22), who in contrast to our observations claimed antiferromagnetic behavior for $CeAl_{1.2}Ge_{0.8}$ with $T_N = 3.4$ K but ferromagnetic behavior for $CeAl_{1.2}Si_{0.2}$, $T_c = 4.2$ K.

$Ce_2Al_3Ge_4$ ($Ba_2Cd_3Bi_4$ type). Temperature and field dependency of the magnetization reveal ferromagnetic order

TABLE 7
Crystallographic Data of $Ce_2Al_3Ge_4$ Quenched from 500°C

Method	Full profile refinement of room temperature X-ray powder diffraction data Number of reflections used in refinement: 408, $20^\circ \leq 2\theta \leq 100^\circ$
Lattice parameters[a]	$a = 0.6078(3)$ nm, $b = 1.5069(9)$ nm, $c = 0.7963(8)$ nm, $V = 0.7294$ nm^3
Structure type	$Ba_2Cd_3Bi_4$
Space group	$Cmca$–D_{2h}^{18}, No. 64, origin at $\bar{1}$, $Z = 4$
Residual values	$R_I = 0.062$, $R_F = 0.051$, $R_P = 0.192$, $R_{wP} = 0.230$

Atom parameters

Atom	Site	x	y	z	B in 10^{-2} nm^2	Occupation
Ce	8f	0	0.1137(1)	0.4169(3)	2.2(2)	1
Ge_1	8f	0	0.1856(2)	0.0529(5)	2.1(3)	1
Al_1	8e	0.25	0.2804(7)	0.25	2.7(5)	1
Ge_2	8e	0.25	0.4512(3)	0.25	2.8(2)	1
Al_2	4a	0	0	0	3.8(6)	1

Interatomic distances (in nm) e.s.d < 0.0008

Central Atom: Ce

Ligand Atom	Distance
Ge_1	0.3094
4 Ge_2	0.3175
2 Ge_2	0.3210
Ge_2	0.3212
2 Al_1	0.3223
2 Ge_1	0.3237
2 Al_1	0.3448
2 Al_2	0.3553
Ce	0.3676

Central Atom: Ge_1

Ligand Atom	Distance
2 Al_1	0.2611
Al_2	0.2829
2 Al_1	0.2897
Ce	0.3094
Ce	0.3211
2 Ce	0.3237

Central Atom: Ge_2

Ligand Atom	Distance
Al_1	0.2574
2 Al_2	0.2611
2 Ge_2	0.3041
2 Ce	0.3175
2 Ce	0.3210

Central Atom: Al_1

Ligand Atom	Distance
Ge_2	0.2574
2 Ge_1	0.2611
2 Ge_1	0.2897
2 Al_1	0.3041
2 Ce	0.3223
2 Ce	0.3448

Central Atom: Al_2

Ligand Atom	Distance
4 Ge_2	0.2611
2 Ge_1	0.2829
4 Ce	0.3553
2 Ce	0.3736

[a] Lattice parameters determined from Guinier film.

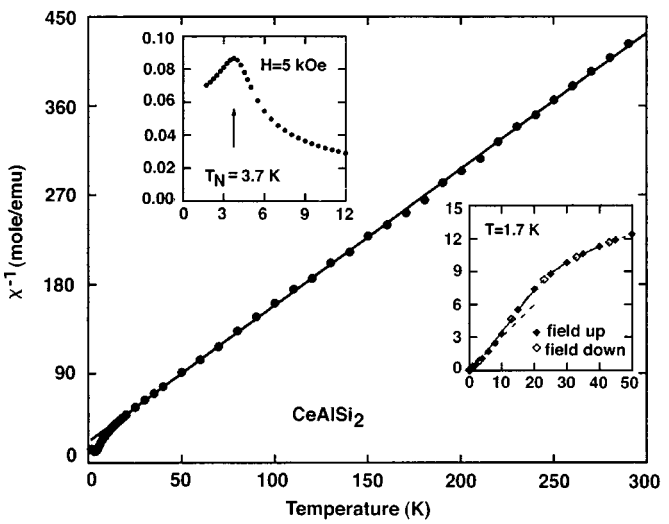

FIG. 7. Temperature variation of the inverse magnetic susceptibility for $CeAlSi_2$. The solid line is a fit of the experimental data to the Curie-Weiss law. Left inset shows the low temperature dependence of the susceptibility measured at 5 kOe. Right inset shows field dependence of the magnetization measured at 1.7 K with increasing magnetic field (filled symbols) and decreasing field (open symbols). The dashed line represents the linear dependency $\sigma(H)$.

below $T_c = 11$ K (Fig. 11). At 50 kOe and 1.7 K the magnetization was 16.5 emu/g, close to magnetic saturation ($\sigma \approx 0.96\ \mu_B$). Above 20 K the magnetic susceptibility is of Curie-Weiss type ($\mu_{eff} = 2.37\ \mu_B$ per Ce atom, $\Theta_P = 9.6$ K). Interesting behavior is encountered in the magnetization curves taken in low fields, namely a rather strong diamagnetic response below 10 K, a feature to be studied in more detail in a forthcoming paper.

TABLE 8
Crystallographic Data of $Ce_2Al_{1.6}Ge_{5.4}$ Quenched from 600°C

Method	Full profile refinement of room temperature X-ray powder diffraction data Number of reflections used in refinement: 840, $20° \le 2\theta \le 100°$
Lattice parameters[a]	$a = 0.8284(3)$ nm, $b = 0.8721(2)$ nm, $c = 1.0767(7)$ nm, $\beta = 101.09(2)°$, $V = 0.7635$ nm^3
Structure type	$La_2Al_{1+x}Ge_{6-x}$
Space group	$C2/m$–C_{2h}^3, No. 12, origin at $\bar{1}$, $Z = 4$
Residual values	$R_I = 0.081$, $R_F = 0.053$, $R_P = 0.171$, $R_{wP} = 0.252$

Atom parameters

Atom	Site	x	y	z	B in 10^{-2} nm^2	Occupation
Ce	8f	0.0850(2)	0.2507(2)	0.3371(1)	0.87(4)	1
$(Ge, Al)_1$	8f	0.2732(5)	0.2104(3)	0.1137(6)	0.54(5)	0.91(1) Ge + 0.09 Al
$(Ge, Al)_2$	4i	0.0602(4)	0	0.1091(5)	1.54(7)	0.77(2) Ge + 0.23 Al
Ge_1	4i	0.1497(3)	0	0.5681(4)	0.37(3)	1
Ge_2	4i	0.3612(4)	0	0.4191(3)	2.88(8)	1
$(Ge, Al)_3$	4i	0.4948(5)	0	0.1196(4)	1.02(4)	0.81(1) Ge + 0.19 Al
Al	4i	0.7859(6)	0	0.1977(7)	0.38(3)	1

Interatomic distances (in nm) e.s.d < 0.0008

Central Atom: Ce

Ligand Atom	Distance
2 Ge_2	0.3125
$(Ge, Al)_1$	0.3151
$(Ge, Al)_1$	0.3164
$(Ge, Al)_2$	0.3166
$(Ge, Al)_1$	0.3211
$(Ge, Al)_2$	0.3224
Ge_1	0.3239
$(Ge, Al)_3$	0.3239
Al	0.3343
Al	0.3368
Ge_2	0.3389

Central Atom: Ge_1

Ligand Atom	Distance
Ge_1	0.2543
Al	0.2545
Ge_2	0.2572
2 Ce	0.3164
2 Ce	0.3211
2 Ce	0.3239

Central Atom: $(Ge, Al)_2$

Ligand Atom	Distance
$(Ge, Al)_2$	0.2470
2 $(Ge, Al)_1$	0.2539
Al	0.2554
2 Ce	0.3224

Central Atom: Al

Ligand Atom	Distance
Ge_1	0.2545
$(Ge, Al)_2$	0.2553
$(Ge, Al)_3$	0.2579
2$(Ge, Al)_1$	0.2651
2 Ce	0.3343
2 Ce	0.3368

Central Atom: $(Ge, Al)_3$

Ligand Atom	Distance
$(Ge, Al)_3$	0.2491
2 $(Ge, Al)_1$	0.2537
Al	0.2579
2 Ce	0.3239

Central Atom: $(Ge, Al)_1$

Ligand Atom	Distance
$(Ge, Al)_1$	0.2463
$(Ge,Al)_3$	0.2537
$(Ge,Al)_2$	0.2539
Al	0.2650
Ce	0.3151
Ce	0.3166

Central Atom: Ge_2

Ligand Atom	Distance
Ge_1	0.2572
Ge_2	0.2619
2 Ce	0.3125
2 Ce	0.3143
2 Ce	0.3389

Second Phase	Small amounts of $Ce_2Al_3Ge_4$
Lattice parameters	$a = 0.6088$ nm, $b = 1.5073$ nm, $c = 0.7969$ nm, $V = 0.7313$ nm^3
Structure type	$Ba_2Cd_3Bi_4$
Space group	$Cmca$–D_{2h}^{18}, No. 64, origin at $\bar{1}$, $Z = 4$
Residual values	$R_I = 0.146$, $R_F = 0.078$

[a] Lattice parameters determined from Guinier film.

$Ce_2Al_{1.6}Ge_{5.4}$ ($La_3Al_{1+x}Ge_{6-x}$ type). A characteristic maximum in the low temperature susceptibility data at a magnetic field of 1 kOe (Fig. 12) indicates antiferromagnetic order below $T_N = 4.7$ K. The weak shoulder in $\chi(T)$ around 10 K is presumably due to a small amount of $Ce_2Al_3Ge_4$. A further argument for the antiferromagnetic ground state

TABLE 9
Crystallographic and EPMA Data of Ternary Ce–Al–Ge Alloys annealed at 600°C

Alloy nominal compositions, at.%	Phase analysis	Structure type	Space group	Unit cell dimensions in nm				EPMA results in at. %			
				a	*b*	*c*	*V* (nm^3)	Ce	Al	Ge	∑m.%
$Ce_{23}Al_7Ge_{70}$	$Ce_2Al_{0.75}Ge_{6.25}$	$La_2Al_{1+x}Ge_{6-x}$[a]	*C2/m*	0.8294(6)	0.8631(7)	1.0748(6)	0.7553	22.6	8.2	69.3	99.7
	Ge	$C_{diamond}$	$Fd\bar{3}m$					0.2	0.2	99.6	106.2
	$Ce_3(Ge, Al)_5$	$GdSi_{2-x}$	*Imma*	0.4342(2)	0.4248(2)	1.4094(7)	0.2600	32.9	3.1	64.0	98.7
$Ce_{18}Al_{21}Ge_{61}$	$Ce_2Al_{1.6}Ge_{5.4}$	$La_2Al_{1+x}Ge_{6-x}$[b]	*C2/m*	0.8349(2)	0.8715(4)	1.0765(7)	0.7690	22.1	14.6	63.3	99.2
	Ge	$C_{diamond}$	$Fd\bar{3}m$					0.2	1.5	98.3	105.6
	$Ce_2Al_3Ge_4$	$Ba_2Cd_3Bi_4$	*Cmca*	0.6096(2)	1.5059(8)	0.7978(5)	0.7324	22.4	31.5	46.1	99.2
$Ce_{24}Al_{34}Ge_{42}$	$Ce_2Al_3Ge_4$	$Ba_2Cd_3Bi_4$	*Cmca*	0.6088(1)	1.5076(5)	0.6879(2)	0.1089	22.1	32.8	45.1	98.7
	$CeAl_2Ge_2$	La_2O_2S	$P\bar{3}m$	0.4272(5)		1.4707(7)	0.2705	19.9	38.6	41.5	98.7
	CeAlGe	$ThSi_2$	$I4_1/amd$	0.4289(2)	0.7979(2)	0.7324		33.6	31.4	35.0	100.0
$Ce_{25}Al_{20}Ge_{55}$	$Ce_2Al_{1.6}Ge_{5.4}$	$La_2Al_{1+x}Ge_{6-x}$[c]	*C2/m*	0.8287(0)	0.8733(4)	1.0746(7)	0.7639	22.4	13.8	63.8	99.9
	$Ce_2Al_3Ge_4$	$Ba_2Cd_3Bi_4$	*Cmca*	0.6081(2)	1.5073(7)	0.7960(4)	0.7296	22.4	31.8	46.0	101.3
	$Ce_3(Ge, Al)_5$	$GdSi_{2-x}$	*Imma*	traces				32.7	4.2	63.0	100.0
$Ce_{40}Al_{15}Ge_{45}$	CeAlGe	$ThSi_2$	$I4_1/amd$	0.4274(1)		1.4666(4)	0.2680	36.9	26.1	37.0	100.6
	$Ce_3(Ge, Al)_5$	$ThSi_2$	$I4_1/amd$	0.4227(0)		1.4328(1)	0.2560	38.9	7.2	53.9	100.1
	CeGe	FeB	*Pnma*	0.8362(6)	0.4086(2)	0.6041(5)	0.2064	51.9	0.6	47.5	100.3
$Ce_{45}Al_{40}Ge_{15}$	$CeAl_2$	Cu_2Mg	$Fd\bar{3}m$	0.8069(1)			0.5253	36.7	63.3	0.0	102.1
	Ce_5Ge_3	Mn_5Si_3	$P6_3/mcm$	0.8873(2)		0.6662(1)	0.4543	64.2	0.7	35.1	100.3
	$Ce(Al_{0.6}Ge_{0.4})_2$	$A1B_2$	*P6/mmm*	0.4346(0)		0.4322(1)	0.0707				
$Ce_{23}Al_{45}Ge_{32}$	CeAlGe	$ThSi_2$	$I4_1/amd$	0.4290(2)		0.6933(3)	0.1101	34.3	31.0	34.8	98.9
	$CeAl_2Ge_2$	La_2O_2S	$P\bar{3}m$	0.4283(2)		0.2708	0.0670	20.2	38.7	41.1	99.3
	Al	Cu	$Fm\bar{3}m$	0.4061(4)	1.4716(3)			0.0	100	0.0	96.0
$Ce_{32}Al_{49}Ge_{19}$	CeAlGe	$ThSi_2$	$I4_1/amd$	0.4318(1)	1.4944(5)	0.2787	0.1713	33.8	44.2	22.0	99.2
	$CeAl_3$	Ni_3Sn	$P6_3/mmc$	0.6548(4)	0.4614(2)			25.1	73.5	1.4	96.9
$Ce_{20}Al_{70}Ge_{10}$	CeAlGe	$ThSi_2$	$I4_1/amd$	0.4285(1)		1.0065(2)	0.5760	33.6	35.5	30.9	97.9
	Ce_3Al_{11}	La_3Al_{11}	*Immm*	0.4396(0)	1.3017(3)	0.2730	0.0665	21.8	77.7	0.5	98.6
	Al	Cu	$Fm\bar{3}m$	0.4051(1)	1.4775(4)			0.2	99.8	0.0	98.3
$Ce_{31}Al_{65}Ge_4$	$CeAl_2$	Cu_2Mg	$Fd\bar{3}m$	0.8061(1)		0.4311(1)	0.1711	34.4	65.6	0	97.4
	$CeAl_3$	Ni_3Sn	$P6_3/mmc$	0.6550(2)	0.4605(3)	0.5239(2)	0.0709	25.2	72.2	2.6	97.5
	$Ce(Al_{0.6}Ge_{0.4})_2$	$A1B_2$	*P6/mmm*	0.4358(2)		0.4311(1)	0.0709	33.8	50.4	15.8	97.0

[a] $\beta = 100.0(1)$.
[b] $\beta = 100.95(6)$.
[c] $\beta = 100.8(2)$.

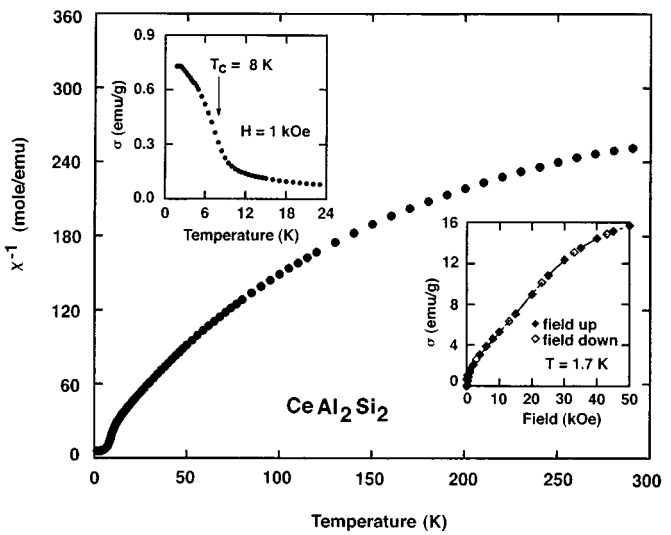

comes from the behavior of the magnetization vs magnetic field, which at 1.7 K varies linearly up to 4 kOe followed by a sharp metamagnetic transition. At 50 kOe the magnetization is 14 emu/g ($\sigma \approx 0.9\ \mu_B$). The deviation below 100 K from paramagnetic Curie-Weiss behavior ($\mu_{eff} = 2.40\ \mu_B$ per Ce-atom, $\Theta_P = -12.5$ K) stems from crystal field effects.

Finally, comparing the magnetic interactions in all the compounds investigated with the interatomic Ce–Ce distances listed in Tables 2 and 4–8, there is no direct correlation visible except for the fact that the highest T_c ($Ce_2Al_3Ge_4$, $T_c = 11$ K) relates to the shortest Ce–Ce distances of 0.3676 nm (Hill-limit ~ 0.32 nm).

FIG. 8. Temperature variation of the inverse magnetic susceptibility for $CeAl_2Si_2$. Left inset shows the low temperature dependence of the magnetization measured at 1 kOe. Right inset shows field dependence of the magnetization measured at 1.7 K with increasing magnetic field (filled symbols) and decreasing field (open symbols).

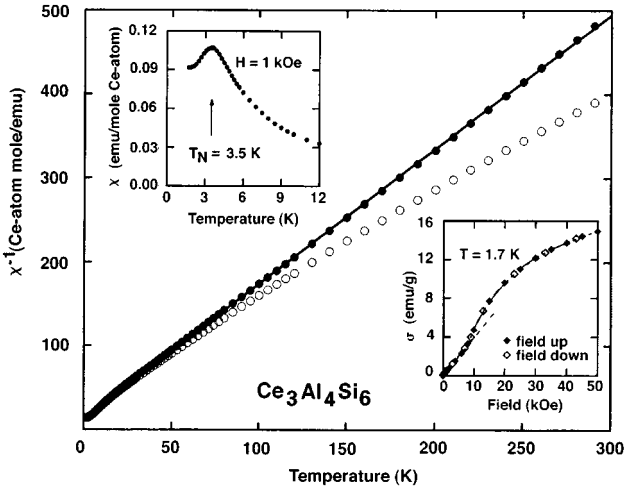

FIG. 9. Temperature variation of the inverse magnetic susceptibility for $Ce_3Al_4Si_6$. The open circles correspond to the raw experimental data and the filled circles are the results corrected for ferromagnetic impurity (see text). The solid line is a fit of the corrected data to the Curie-Weiss law. Left inset shows the low temperature dependence of the susceptibility measured at 1 kOe. Right inset shows field dependence of the magnetization measured at 1.7 K with increasing magnetic field (filled symbols) and decreasing field (open symbols). The dashed line represents the linear dependency $\sigma(H)$.

D. Electrical Resistivity

The electrical transport behavior of the cerium-aluminium-silicides and -germanides is summarized in Fig. 13.

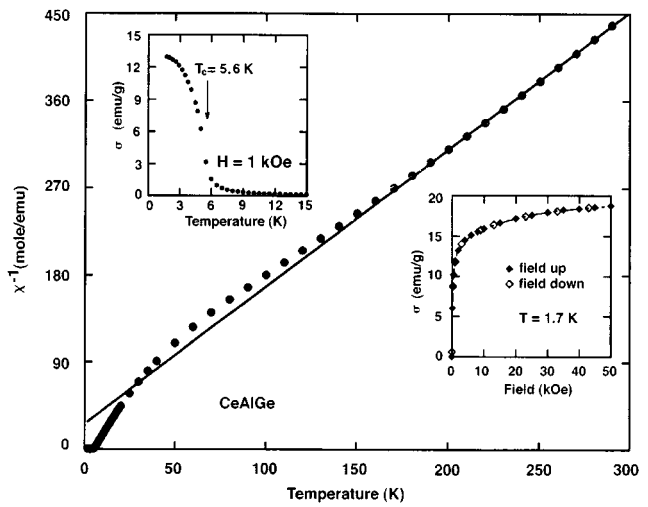

FIG. 10. Temperature variation of the inverse magnetic susceptibility for CeAlGe. The solid line is a fit of the experimental data to the Curie-Weiss law. Left inset shows the low temperature dependence of the magnetization measured at 1 kOe. Right inset shows field dependence of the magnetization measured at 1.7 K with increasing magnetic field (filled symbols) and decreasing field (open symbols).

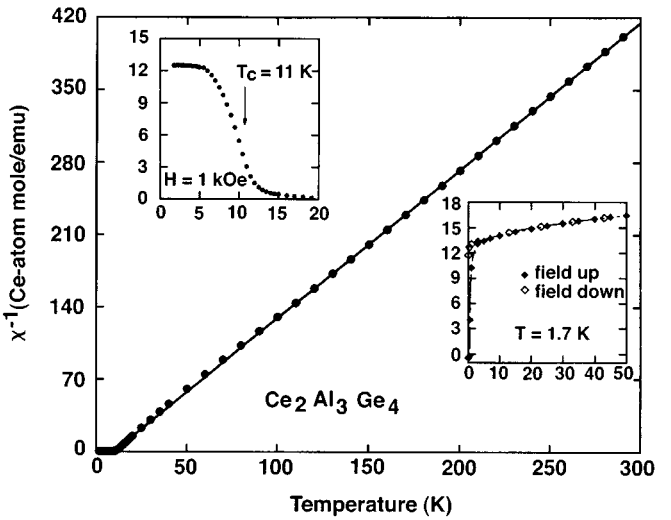

FIG. 11. Temperature variation of the inverse magnetic susceptibility for $Ce_2Al_3Ge_4$. The solid line is a fit of the experimental data to the Curie-Weiss law. Left inset shows the low temperature dependence of the magnetization measured at 1 kOe. Right inset shows field dependence of the magnetization measured at 1.7 K with increasing magnetic field (filled symbols) and decreasing field (open symbols).

The curvature in $\rho(T)$ is typical for intermetallic cerium compounds exhibiting crystal field interactions below about 150 K. The sharp dropoff of the resistivity at low temperatures observed for $Ce_2Al_3Ge_4$ and $Ce_2Al_{1.6}Ge_{5.4}$ confirms the magnetic ordering temperatures derived from the magnetic measurements.

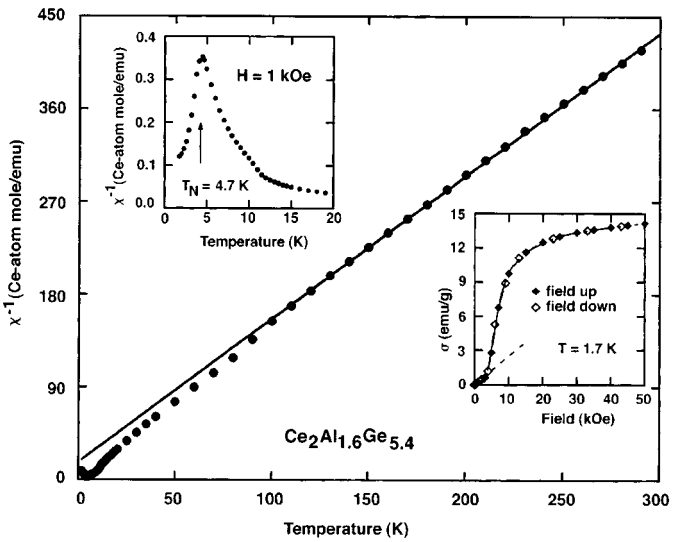

FIG. 12. Temperature variation of the inverse magnetic susceptibility for $Ce_2Al_{1.6}Ge_{5.4}$. The solid line is a fit of the experimental data to the Curie-Weiss law. Left inset shows the low temperature dependence of the susceptibility measured at 1 kOe. Right inset shows field dependence of the magnetization measured at 1.7 K with increasing magnetic field (filled symbols) and decreasing field (open symbols). The dashed line represents the linear dependency $\sigma(H)$.

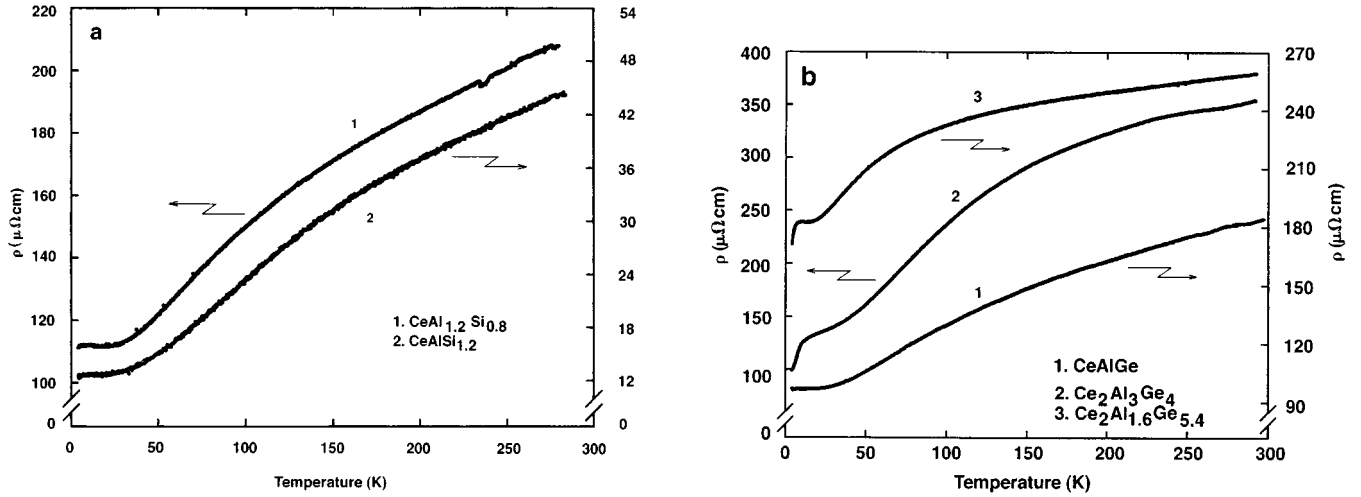

FIG. 13. Temperature dependence of the electrical resistivity for (a) $CeAl_{1.2}Si_{0.8}$ and $CeAlSi_2$, and (b) CeAlGe, $Ce_2Al_3Ge_4$, and $Ce_2Al_{1.6}Ge_{5.4}$.

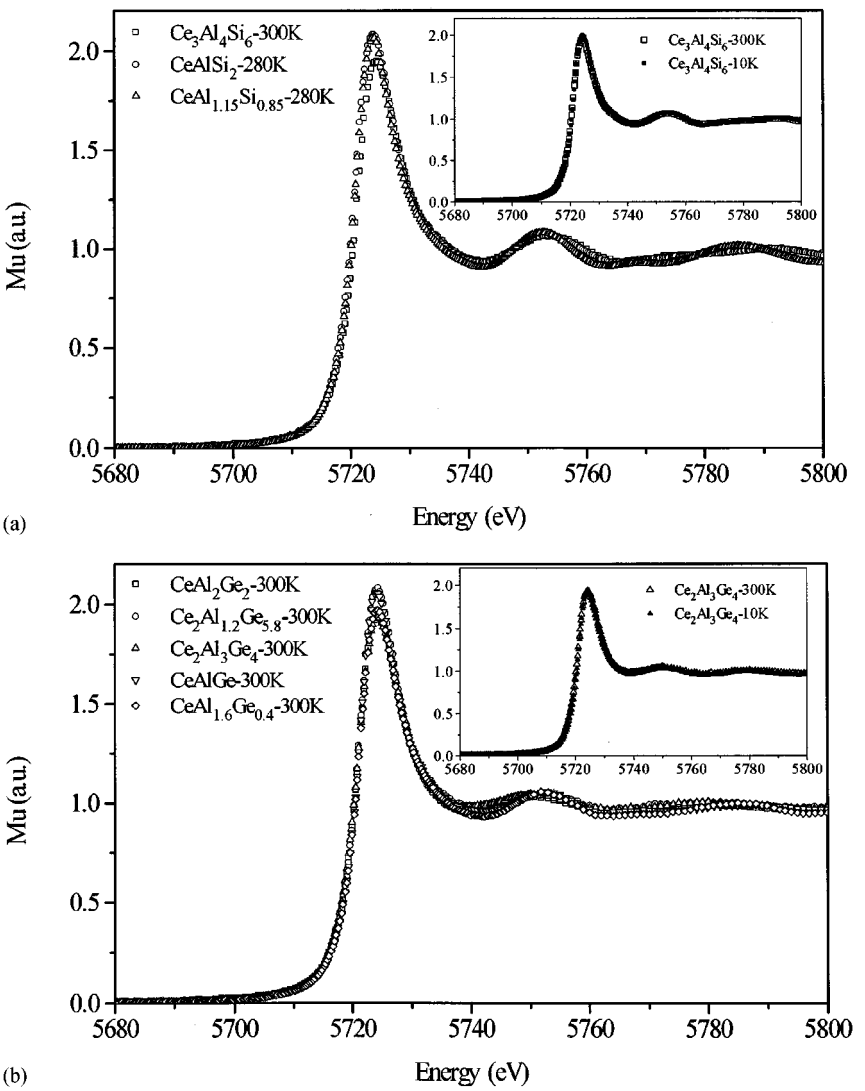

FIG. 14. X-ray absorption spectra for the various cerium-aluminium-silicides and -germanides at 10 K and room temperature.

E. X-Ray Absorption Spectroscopy

XAS measurements were performed at 10 K and room temperature. Data in all cases are consistent with a stable trivalent cerium ground state $^2F_{5/2}$. No significant difference was observed in the spectra at 10 K and room temperature, as shown for $Ce_3Al_4Si_6$ and $Ce_2Al_3Ge_4$ (Fig. 14).

ACKNOWLEDGMENTS

This research has been sponsored in part by the FFWF-P8218 as part of EU–Human Capital and Mobility Project ERBCHRX-CT93-0284. P.R. and D.K. are grateful to the Austrian–Polish Scientific Technical Exchange Program (Project 6) for research stipends in Vienna and Wroclaw.

REFERENCES

1. G. Brauer and H. Haag, *Z. anorg. Chemie* **267,** 198 (1952).
2. L. N. Altunina, E. I. Gladyshevskij, O. S. Zarechnyuk, and I. F. Kolobnev, *Zhur. Neorg. Khim.* **8,** 1673 (1963).
3. O. S. Zarechnyuk, Zb. Robit Aspirantiv, L'vivs'k. Univ., Prirodn., Nauk, Lvov, 15–20 (1963).
4. A. Raman, *Z. Metallkunde* **58,** 179 (1967).
5. A. Raman and H. Steinfink, *Inorg. Chem.* **6,** 1789 (1967).
6. A. A. Murav'eva, O. S. Zarechnyuk, and E. I. Gladyshevskij, Visn. L'viv. Derz. Univ. Ser. Khim. **13,** 14 (1972).
7. A. A. Murav'eva, "Autoreferat Dis. Kand. Khim.," abstract of thesis, Nauk. Lvov, 1–18 (1972).
8. P. Rogl, *in* "Ternary Alloys" (G. Petzow and G. Effenberg, Eds.), Vol. 4, pp. 100–103. VCH, Germany, 1991.
9. H. Flandorfer and P. Rogl, *J. Solid State Chem.* **27,** 308 (1996).
10. R. Schmid-Fetzer, *in* "Ternary Alloys" (G. Petzow and G. Effenberg, Eds.), Vol. 4, pp. 67–70. VCH, Germany, 1991.
11. A. A. Murav'eva and O. S. Zarechnyuk, *Inorg. Mater.* **6,** 933 (1970).
12. O. S. Zarechnyuk, A. A. Murav'eva, and E. I. Gladyshevsky, *Dopov. Akad. Nauk Ukr. RSR* **A8,** 753 (1970).
13. J. T. Zhao and E. Parthé, *Acta Crystallogr. Sect. C* **46,** 2276 (1990).
14. J. T. Zhao, K. Cenzual, and E. Parthé, *Acta Crystallogr. Sect. C* **47,** 1777 (1991).
15. J. T. Zhao and E. Parthé, *Acta Crystallogr. Sect. C* **47,** 1781 (1991).
16. R. Goldstein, D. E. Newbury, P. Echlin, D. C. Joy, C. E. Fiori, and E. Lifshin, "Scanning Electron Microscopy and X-ray Microanalysis," Chap. 7, p. 305, Plenum Press, New York, 1981.
17. H. Flandorfer, A. Kostikas, P. Rogl, C. Godart, M. Giovannini, A. Saccone, and R. Ferro, *J. Alloys Compds.* **240,** 116 (1996).
18. D. Bonnin, P. Kaiser, J. Desbarres, and C. Fretigny, "Structure fines d'absorption des rayons X," Ecole CNRS, Garchy, France, 1988.
19. J. Roehler, *J. Magn. Magn. Mater.* **47, 48,** 175 (1985).
20. T. B. Massalski, "Binary Alloy Phase Diagrams," 2nd ed. ASM International, Materials Park, OH, 1990.
21. S. K. Dhar, S. M. Pattalwar, and R. Vijayaraghavan, *J. Magn. Magn. Mater.* **104–107,** 1303 (1992).
22. S. K. Dhar and S. M. Pattalwar, *J. Magn. Magn. Mater.* **152,** 22 (1996).